Ab initio Molecular and Solid State Studies of the Fe^{II} Spin Cross-over System [Fe(btz)₂(NCS)₂] (btz = 2.2'-bis-4.5-dihydrothiazine)

Lara Kabalan^a, Samir F. Matar^a, Mirvat Zakhour^b, and Jean François Létard^a

^a ICMCB, CNRS, Université Bordeaux 1. 87 Avenue du Dr. Albert Schweitzer, F-33608 Pessac Cedex, France

^b LCPM, Université Libanaise, Fanar-Beyrouth, Lebanon

Reprint requests to S. F. Matar. E-mail:matar@icmcb-bordeaux.cnrs.fr

Z. Naturforsch. 2008, 63b, 154-160; received October 12, 2007

Ab initio computations within the density functional theory are reported for the spin cross-over complex [Fe(btz)₂(NCS)₂] (btz = 2.2'-bis-4.5-dihydrothiazine), where $3d^6$ Fe^{II} is characterized by high-spin (HS t_{2g}^4 , e_g^2) and low-spin (LS t_{2g}^6 , e_g^0) states. Results of infrared and Raman spectra for the isolated molecule are complemented for the crystalline solid with a full account of the electronic band structure properties: the density of states assessing the crystal field effects and the chemical bonding, assigning a specific role to the Fe–N interactions within the coordination sphere of Fe^{II}.

Key words: Density Functional Theory, Spin Cross-over (SCO)

Introduction

Inorganic transition metal ion complexes may exhibit two electronic states of the d electrons, the highspin (HS) and low-spin (LS). Switching between these two states is associated with small energy changes around $\sim k_{\rm BT}$, and the transitions can be achieved with external constraints such as temperature, pressure as well as light. Such spin cross-over (SCO) behavior has been discussed in detail in several reviews [1-4]. Theoretical studies at the molecular level [5, 6] are equally available but to our knowledge there are no solid state investigations of the electronic structure for the whole crystal system. Such studies are likely to provide further information on the changes of the electronic density of states as well as on the chemical bonding in the close neighborhood of the central Fe ion. The purpose of this work is to provide spectroscopic and electronic structure information on the SCO system [Fe(btz)₂(NCS)₂], both for the isolated molecule and for the extended solid state. The btz ligand is similar in its structure to the 2,2'-bipyridine ligand. However, the presence of sulfur provides a non-planar bidentate ligand as it is shown in Fig. 1. The mono-dentate NCS⁻ ligands are in a cis-position like in most SCO complexes, such as $[Fe(phen)_2(NCS)_2]$ [7].

Crystallographic and SCO characteristics were investigated by many authors [8-10]. Crystals of the prototype of SCO systems, such as

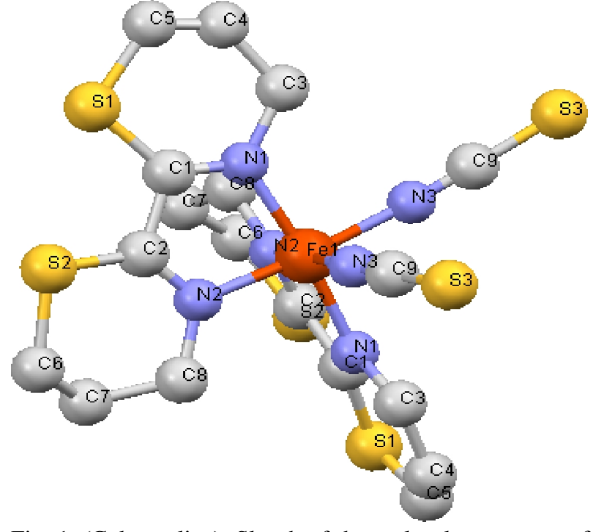


Fig. 1. (Color online). Sketch of the molecular structure of the SCO complex [Fe(btz)₂(NCS)₂] as obtained from X-ray crytallography [8, 9]. Hydrogen atoms not shown for clarity.

[Fe(phen)₂(NCS)₂], keep the orthorhombic space group (*Pbcn*, No. 60) during the spin transition, the cell parameters remaining closely similar and the molecular packing unchanged. In the case of [Fe(btz)₂(NCS)₂], the SCO transition is also not accompanied by a structural transition. This underlines a coupling of different nature and the importance of packing aspects between close molecules [11].

0932-0776 / 08 / 0200-0154 \$ 06.00 © 2008 Verlag der Zeitschrift für Naturforschung, Tübingen · http://znaturforsch.com

Contrary to $[Fe(phen)_2(NCS)_2]$, the SCO transition in $[Fe(btz)_2(NCS)_2]$ is gradual and $T_{1/2}$, which is the so-called equilibrium temperature of the system, is about 215 K [12].

Theoretical and Computational Frameworks

Although the use of the Hartree-Fock (HF) approach has been shown to provide a good description of the molecular orbital and chemical bonding properties, mainly in organic chemistry, it is now recognized that the density functional theory (DFT) framework [13] brings far more accurate results regarding the energetics and related properties. This is because the compulsory exchange and correlation (XC) effects are equally treated, albeit at a local level, within DFT, while only the exchange is well accounted for in HF although in a better way (exact exchange [14]) than in DFT. Taking the best out of each one of the two approaches led to improvements in ab initio molecular calculations with the so called "hybrid functionals". They consist of mixing exact HF exchange, following Becke [14], and DFT based correlations following Lee, Yang and Parr, i. e., the so-called LYP correlation [15], with proportions that help to reproduce molecular properties of several systems. In this work, the calculations were performed using the GAUSSIAN 03 package [16].

In the solid state the molecule is packed within the framework of an extended solid, as revealed by an X-ray diffraction crystal structure determination [8, 9]. This allows for a better account of possible intermolecular effects and for a description of the electronic band structure of the whole system. For this purpose we use the all electron augmented spherical wave method (ASW) [17]. Beside its use of DFT, the ASW method is based on the atomic sphere approximation (ASA), a special form of muffin-tin approximation dividing the cell volume into atomic spheres whose total volume is equal to the cell volume. The calculation being carried out in the atomic spheres' space, empty spheres (pseudo-atoms) need to be introduced (without symmetry breaking) in open (low compactness) structures such as that of the system studied here. Further, empty spheres allow for the iono-covalent characteristics of the system to be accounted for by receiving charges from actual atomic species. The use of this method in molecular systems has been validated by Eyert et al. [18]. In the context of the present study, ASW-LDA was used in order to obtain a description of the electronic structure with the partial, site-projected

Table 1. Distances (Å) and angles (deg) obtained by using the LanL2DZ basis set and the B3LYP hybrid functional for the geometry optimization in LS and HS [Fe(btz)₂(NCS)₂] in comparison with experiment. Average $\langle d_{\text{Fe}--\text{N}} \rangle$ distances are provided for comparison (see text)^a.

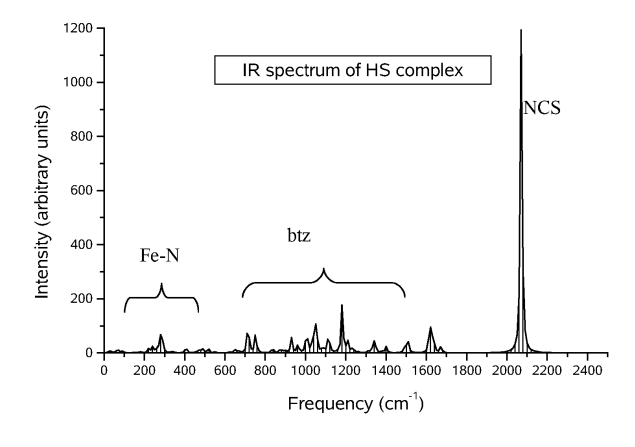
'	LS	LS _{exp}	HS	HS _{exp}
d_{FeNCS}	1.979	1.947	2.085	2.066
$d_{\text{Fe}N(\text{btz})}$	1.987	1.967	2.267	2.177
$d_{\text{Fe}\text{N(btz)}}$	2.005	1.972	2.207	2.166
α(Fe–N–C)	155.20	169.1	145.30	167.80
α (NCS)-Fe-(NCS)	96.132	86.06	107.72	91.53
$\alpha(N_{btz})$ -Fe- (N_{btz})	80.0	80.0	73.92	74.7
$\langle d_{\mathrm{FeN}} \rangle$	1.970	1.961	2.186	2.136

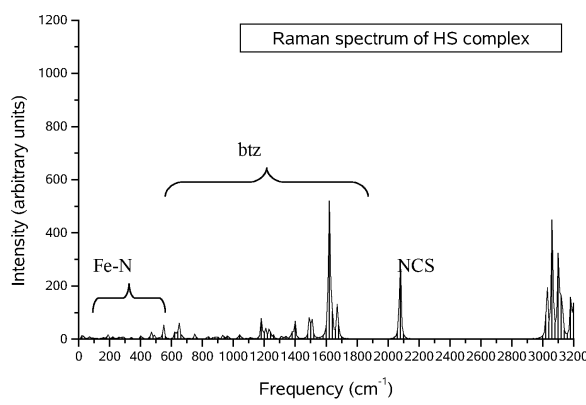
^a Experimental values taken from ref. [8, 9].

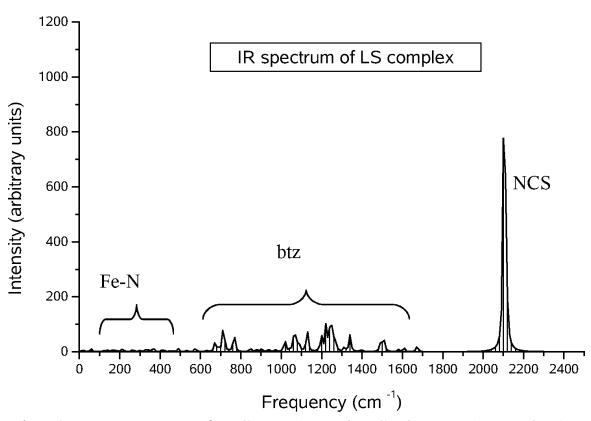
density of states. Further, the chemical interaction was assessed especially within the coordination sphere of divalent iron from $E_{\rm COV}$ (energy of covalent bond), which allows to get two-body chemical bond characteristics [19]. Negative, positive and zero $E_{\rm COV}$ values point to bonding, anti-bonding and non-bonding interactions, respectively.

Results and Discussion for the Isolated Molecule

Starting geometries for molecules in HS and LS configuration were extracted from the CIF files (Crystallographic Information File) [8,9]. After testing different functionals and basis sets through preliminary trial computations, we found most accurate results for the energy and vibrational spectra in LS and HS states with the hybrid functionals B3LYP 6-31G together with 6-311G as well as LanL2DZ basis sets (Table 1). The latter include double- ζ with the Los Alamos effective core potential for Fe and S atoms and the Dunning-Huzinaga all-electrons double- ζ basis set with polarization functions for H, C, and N atoms (ζ is the exponent in the Gaussian-type orbitals GTO) [20,21]. First, the geometry of the molecule was optimized in both spin states and the results tested against the experimental distances within the coordination sphere of iron (Fig. 1). Table 1 gives the obtained distances and angles for the LS and HS configuration from B3LYP/LanL2DZ calculations; however, we note that close values were equally obtained with the 6-311G basis set. Although the final Fe-N distances do not show a perfect octahedral environment, we find average d_{LS} (Fe–N) ~ 1.990 Å, smaller than d_{HS} (Fe–N) ~ 2.186 Å. This is an expected result due to the increase of the volume of the divalent Fe coordination sphere arising from the occupation of anti-bonding e_g^* states with two unpaired electrons: LS $(t_{2g}^6 e_g^0)$; HS $(t_{2g}^4 e_g^2)$. These average values agree with theoretical







1200

1000

Raman spectrum of LS complex

Fig. 2. IR spectra of HS (top) and LS (bottom) [Fe(btz) $_2$ -(NCS) $_2$] calculated with the LanL2DZ basis set.

Fig. 3. Raman spectra of HS (top) and LS (bottom) of [Fe(btz)₂(NCS)₂] calculated with the LanL2DZ basis set.

Frequency (cm⁻¹)

ones for similar SCO complexes in the literature [6], where the BP86 hybrid functional and the triple- ζ basis set were used. Similarly, an agreement between computed and experimental values was also found. However, some discrepancy was observed for the magnitudes of [(Fe-N-C)] and [((SCN)-Fe-(NCS))] angles, not only with the LanL2DZ basis set but also with all other basis sets employed. From the geometryoptimized configurations with B3LYP/LanL2DZ, the theoretical infra-red (IR) and Raman spectra were computed for the purpose of providing a spectroscopic signature of the system in its two spin states. The differences that can be observed for the positions as well as for the relative intensities between IR bands and Raman lines in both HS and LS states point to the fact that there are active modes in IR which are inactive in Raman spectroscopy, and *vice versa* (Figs. 2 and 3).

cuss the domain of low frequencies. At $v < 500 \text{ cm}^{-1}$ the Fe-N elongation modes are present. In the case of LS, a peak at 532.1 cm⁻¹ could be detected and assigned to the Fe-N_(NCS) elongation which is mainly active in IR. This magnitude comes close to that of the experimental value of 532.6 cm⁻¹ [3,6]. For the HS case this same elongation is found at $v = 240.7 \text{ cm}^{-1}$ (exp. 249.0 ${\rm cm}^{-1}$ [3,6]). Fe–N_(btz) HS/LS elongation values are 221/367 cm⁻¹, following the same trend. The other relevant frequencies characterizing the HS/LS varieties which could serve as a signature are those of the NCS- ligand; their magnitudes and assignments are given together with experimental results in Table 2. Values for the LS state are systematically higher than for the HS state which can be understood if one considers elementary citeria such as the average distances which are shorter for the LS complex (Table 1). The frequency of the electromagnetic wave which induces the vibration of elongation is given by

From this we have spectrocopic signatures for the systems not only at the level of the spin states (LS/HS) but also for the IR/Raman frequencies. First, we dis-

Table 2. Comparison of antisymmetric and symmetric N-C-S frequencies (in cm⁻¹) between LS and HS [Fe(btz)₂(NCS)₂]. Experimental values taken from ref. [3, 6] are given in parentheses.

IR (LS)	Raman (LS)	IR (HS)	Raman (HS)
2103.89 (2100)	2103.89 (2107)	2070.71 (2060)	2070.71 (2062)
2113.51 (2110)	2113.51 (2110)	2077.78 (2070)	2077.78 (2072)

the relation $v=\frac{1}{2\pi}\sqrt{\frac{k}{\mu}}$ where k is the constant of the bonding strength (considered here as a spring), proportional to the binding energy and μ , the reduced mass of the two atoms connected by this bond. The distances in the case of LS are smaller than in the HS case; thus the ratio $k\frac{\text{HS}}{\text{LS}}=0.962$ for the symmetric NCS elongation, has a magnitude lower than 1.

At this stage of development of the results, it becomes relevant to discuss the energetics, $\Delta_{LS/HS}$ (i.e., $\Delta_{\rm HS} - \Delta_{\rm LS}$), between the two spin states with the functional and basis set used. The average value obtained for $\Delta_{\rm HS/LS}$ is ~ -2.5 kJ/mol, favoring the high-spin case. We note that $\Delta_{LS/HS}$ is governed by the amount of exchange admixture in the energy functional [22, 23]. A main result was that an adjustment of the exact exchange admixture is necessary since pure density functionals tend to favor low-spin states, while hybrid functionals like B3LYP usually give the high-spin state as the lowest-energy state if the low-spin/high-spin energy splitting $\Delta_{LS/HS}$ is not too large [24]. Our results are in agreement with those of Paulsen, Trautwein and co-workers [5] who have conducted an extensive study on several spin cross-over complexes using different basis sets and density functionals. Their results show that B3LYP favors, in general, the high-spin state while all pure density functionals favor the low-spin state. Interestingly, we shall show that the energetics extracted from the solid state calculations (below) exhibit this tendency.

Further we have tried to reproduce the equilibrium temperature of the system $T_{1/2}$. At the transition, equal proportions of HS and LS populations are co-existing and one defines $T_{1/2}$ from $\Delta G = \Delta H - T\Delta S$, where G, H and S indicate free enthalpy, enthalpy and entropy. At this equilibrium, $\Delta G = 0$, and T leads to $T_{1/2}$ defined as $\frac{\Delta H_{T1/2}}{\Delta S_{T1/2}}$ with $\Delta S = \Delta S_{\rm el} + \Delta S_{\rm vib} + \Delta S_{\rm rot} + \Delta S_{\rm trans}$. Notice that in this model the translational contribution would be the same for both spin states and thus it needs not be taken into account. The electronic contribution to the entropy arises from the HS configuration because $\Delta S_{\rm el} = R[\ln(2s+1)_{\rm HS} - \ln(2s+1)_{\rm LS}]$. We

designate total spins by script s in order to differenciate from entropy S; further, $R=8.3 \text{ J mol}^{-1} \text{ K}^{-1}$. For LS all spins are paired in the t_{2g} manifold t_{2g}^6 , hence s=0, while for HS s=2. With these s values we arrive at $\Delta S_{\text{el}}=R\ln(2s_{\text{HS}}+1)=13.38 \text{ J mol}^{-1} \text{ K}^{-1}$. This is the same result as required by theory where we must assume that the electronically excited states are so much higher in energy that they cannot be excited thermally [6]. Adding ΔS_{el} to ΔS_{vib} and ΔS_{rot} gives $T_{1/2}\sim 100 \text{ K}$ which is about half the experimental value (215 K). Such a discrepancy also arises in calculations on a single molecule such as [Fe(phen)₂(NCS)₂] for which a magnitude of 1530 K ($T_{1/2}(\exp.) = 176 \text{ K}$ [7]) was obtained in the literature with the BP86 hybrid functional [22].

One can interpret the reduced $T_{1/2}$ value by the fact that we have a calculated $\Delta H = 6.4$ kJ mol $^{-1}$ while the magnitude we extract from the experimental magnetic susceptibility in the $\chi_{\rm M}$ $T={\rm f}(T)$ curve [11] amounts to 15 kJ mol $^{-1}$. Applying the thermodynamic relation $\Delta G = \Delta H - T\Delta S$ which gives $\Delta S = 64$ J mol $^{-1}$ K $^{-1}$, while it is 66 with the 6-31g basis-set calculations, we can conclude that the problem stems from ΔH . This raises modeling problems in reproducing experimental magnitudes of $T_{1/2}$ which can have several origins, one being the packing effects which call for the use of neighboring molecular species besides the single isolated molecule. We expect improvements of $T_{1/2}$ provided such neighboring molecules are adjoined to the complex. These calculations are underway.

Calculations for the Extended Solid

To gain insight into the role of each atomic species in the electronic band structure and into the chemical bonding, we carried out all electrons, spin degenerate calculations for the tetra-molecular [Fe(btz)₂(NCS)₂] system with the experimental data in the orthorhombic space group Pbcn (No. 60) [8,9] (Fig. 4). Our calculations show large charge transfer, transferring ionic charge from the atoms Fe, N, C and S to the empty spheres (ES). One should remember that ES are pseudo-atoms with zero-core, introduced as stated above to account for the large voids within the open structure of the molecular system. The plots of the projected density of states (PDOS) for the constituent atom sites are presented in Figs. 5 and 6 for the LS and HS configurations, respectively. Along the x axis, the energies are considered with respect to the top of the valence band VB (E_V) , not the Fermi energy (E_F) ,

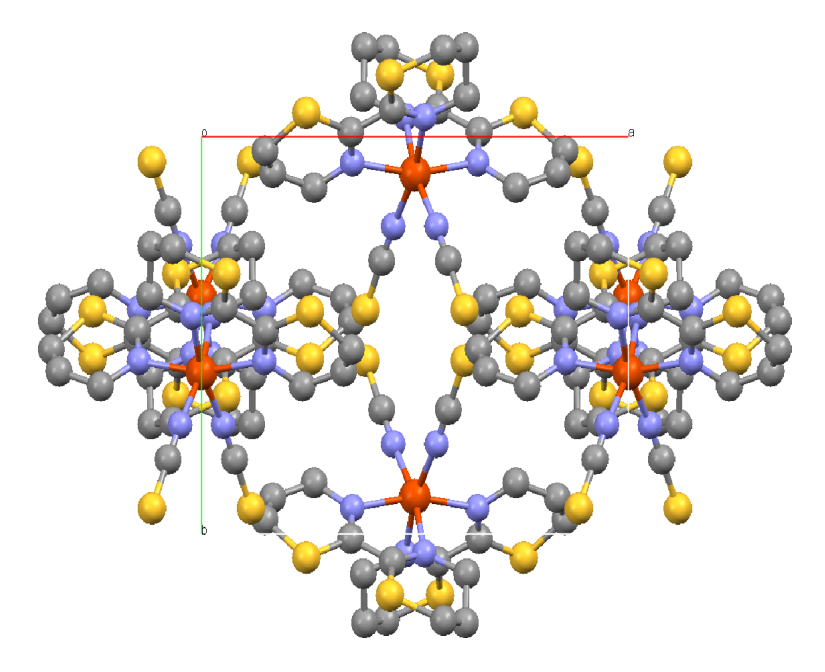


Fig 4. (Color online) Crystal structure of tetra-molecular [Fe(btz)2(NCS)2] as projected onto the ab plane. Atoms: Fe (red), N(blue), C (grey), S (yellow). Hydrogen atoms not shown for clarity.

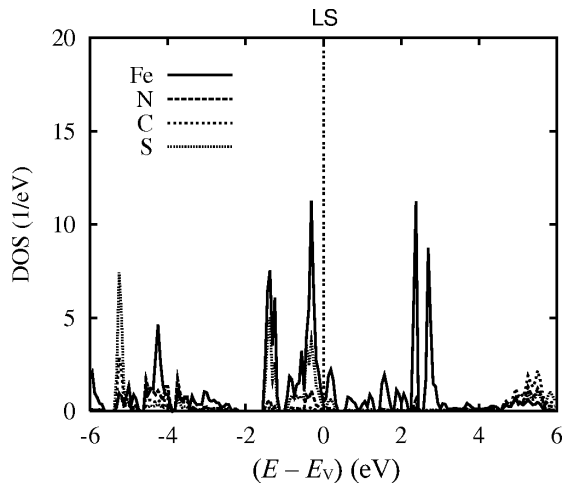
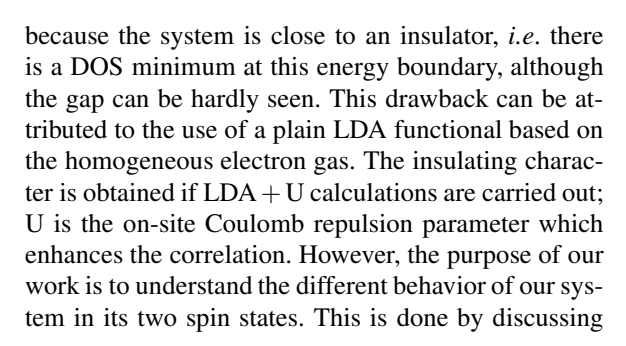


Fig. 5. Site projected density of states (PDOS) of LS [Fe(btz)₂(NCS)₂]. The energy reference is the top of the va-



lence band (E_{V}) .

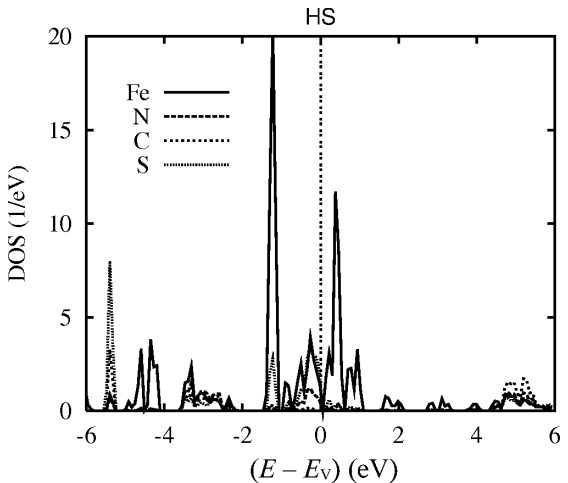


Fig. 6. Site projected density of states (PDOS) of HS $[Fe(btz)_2(NCS)_2]$. The energy reference is the top of the valence band (E_{V}) .

the PDOSs which are most significant in the neighborhood of E_V . For this reason we consider a narrow energy window near -6, 6 eV with a dominant presence of Fe PDOS (solid lines) on both sides of E_V . Chemical bonding of Fe atoms with other atoms, especially N, is observed in the lower part of the VB. The interesting feature which can be traced out from the PDOS is relevant to the intrinsic properties of the complex system in the LS and HS states. The major difference between Figs. 5 and 6 is the splitting of Fe (d) states accord-

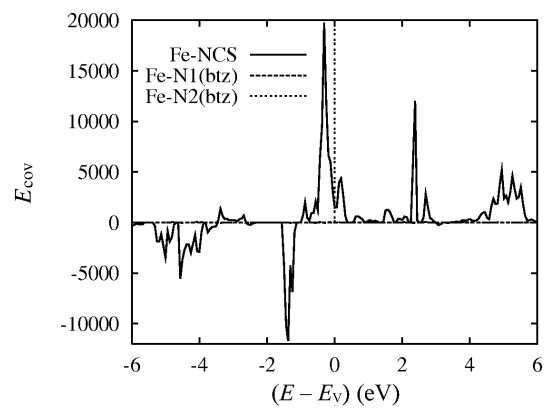


Fig. 7. Chemical bonding following the $E_{\rm COV}$ criterion (arbitrary units) for the different Fe–N interations within [Fe(btz)₂(NCS)₂] in the low-spin (LS) case. Energy reference is the top of the valence band ($E_{\rm V}$).

ing to the crystal field expected for LS and HS, *i.e.* the empty e_g -like manifold PDOSs are high in energy within the conduction band (CB) (Fig. 5) in LS with a separation of ~ 2.5 eV or 242 kJ mol⁻¹, which comes close to a typical crystal field splitting magnitude Δ_0 in octahedral environments. On the contrary, the partially filled HS e_g -like manifold is close to E_V (Fig. 6).

The variational energy difference between results of HS and LS ASW-LDA calculations carried out with the same Brillouin zone k mesh precision amounts to $\Delta E_{\rm LS/HS} = +8374.6$ J for 4 formula units (fu), i.e., +2.09 kJ per fu. This favors the LS configuration energetically, contrary to all molecular calculations above.

Regarding the chemical bonding within the complex system one mainly needs to examine the bonds which reveal the variation at the transition, *i. e.* the Fe-N bonds. Considering the LS configuration (the same reasoning holds for HS), Table 1 gives distances $d_{\text{Fe-NCS}} = 1.979 \text{ Å}$ shorter than distances $d_{\text{Fe-N(btz)}}$

(1.987 and 2.005 Å). Thus one expects relatively stronger bonding for the former. The $E_{\rm COV}$ plots shown in Fig. 7 exhibit a mainly bonding Fe–N character within the VB. However, there is the striking feature of a largely dominant Fe–N_{NCS} interaction as it is implied by the formula "Fe²⁺(NCS⁻)₂"(btz)₂, *i. e.* the major bonding interaction is due to the charged ligands only while the btz ligand plays only a secondary role in the coordination sphere of Fe²⁺ with respect to bonding.

Conclusion

In this work, we presented results of a DFT calculation for the [Fe(btz)₂(NCS)₂] complex. The change of the metal-ligand bond lengths upon a spin-flip from singlet to quintet which is rationalized in terms of a one-particle picture as an occupation of molecular orbitals with anti-bonding character is well-reproduced at the level of the single molecule. The calculated IR and Raman spectra for the low-spin and high-spin states obtained with the LanL2DZ frequency of the antisymmetric and symmetric NCS elongations are very close to those obtained experimentally. We also carried out calculations for the solid state accounting for a crystalline tetra-molecular model complex. With the all-electron ASW-DFT method we obtained the PDOS in the two states and the iron chemical bonding characteristics. The change in the anti-bonding e_g^* from LS to HS is due to the NCS ligand approach. The chemical bonding E_{COV} reflects the predominance of the Fe²⁺–NCS[–] bonds as compared to the Fe–N bonds to the neutral btz ligand.

Acknowledgements

Lara Kabalan thanks the CNRSL, Lebanese Council of Research, for her Ph.D. scholarship. We acknowledge computational facilities provided by the University Bordeaux 1 within the M3PEC Mésocentre Régional (http://www.m3pec.u-bordeaux1.fr) supercomputers.

- [1] P. Gütlich, Y. Garcia, H. Goodwin, Am. Chem. Soc. Rev. 2000, 29, 419 – 427.
- [2] P. Gütlich, H. A. Goodwin (Eds.), Spin Crossover in Transition Metal Compounds III, Topics in Current Chemistry, Vol. 235, Springer, Berlin, Heidelberg, 2004.
- [3] P. Gütlich, Structure and Bonding, 1981, 44, 83 195.
- [4] J. F. Létard, P. Guionneau, L. Goux-Capes in Spin Crossover in Transition Metal Compounds III, Topics in Current Chemistry, Vol. 235 (Eds. P. Gütlich, H. A. Goodwin), Springer, Berlin, Heidelberg, 2004, pp. 221–249.
- [5] H. Paulsen, L. Duelund, H. Toftlund, A. Trautwein, *Inorg. Chem.* 2001, 40, 2201 2203.
- [6] C. Brehm, M. Reiher, S. Schneider, J. Phys. Chem. A, 2002, 106, 12024.
- [7] B. Gallois, J. A. Real, C. Hauw, J. Zarembowitch, *Inorg. Chem.* 1990, 29, 1152.
- [8] J. A. Real, B. Gallois, T. Granier, F. Suez-Panama, J. Zarembowitch, *Inorg. Chem.* 1992, 31, 4972 – 4979.
- [9] T. Granier, B. Gallois, J. A. Real, J. Gaultier, J. Zarembowitch, *Inorg. Chem.* 1993, 32, 5305 – 5312.
- [10] T. Granier, B. Gallois, J. A. Real, J. Gaultier, J. Zarembowitch, *Inorg. Chem.* 2004, 32, 221 – 249.

- [11] F. Suez-Panama-Bouto, Ph. D. Thesis, Université Bordeaux, Bordeaux, 1991.
- [12] P. Guionneau, M. Marchivie, G. Bravic, J. F. Létard, D. Chasseau, in *Spin Crossover in Transition Metal Compounds II, Topics in Current Chemistry*, Vol. 234 (Eds. P. Gütlich, H. A. Goodwin), Springer, Berlin, Heidelberg, 2004, pp. 97 – 128.
- P. Honenberg, W. Kohn, *Phys. Rev.* **1964**, *136*, B864;
 W. Kohn, L. J. Sham, *Phys. Rev.* **1965**, *140*, A1133.
- [14] V. D. Becke, J. Chem. Phys. 1988, 88, 2547.
- [15] C. Lee, W. Yang, R. G. Parr, Phys. Rev. 1988, B37, 785.
- [16] M. J. Frisch, G. W. Trucks, H. B. Schlegel, G. E. Scuseria, M. A. Robb, J. R. Cheeseman, J. A. Montgomery, Jr., T. Vreven, K. N. Kudin, J. C. Burant, J. M. Millam, S. S. Iyengar, J. Tomasi, V. Barone, B. Mennucci, M. Cossi, G. Scalmani, N. Rega, G. A. Petersson, H. Nakatsuji, M. Hada, M. Ehara, K. Toyota, R. Fukuda, J. Hasegawa, M. Ishida, T. Nakajima, Y. Honda, O. Kitao, H. Nakai, M. Klene, X. Li, J. E. Knox, H. P. Hratchian, J. B. Cross, V. Bakken, C. Adamo, J. Jaramillo, R. Gomperts, R. E. Stratmann, O. Yazyev, A. J. Austin, R. Cammi, C. Pomelli, J. W. Ochterski, P. Y. Ayala, K. Morokuma, G. A. Voth, P. Salvador, J. J. Dannenberg, V. G. Zakrzewski, S. Dapprich, A. D. Daniels, M. C. Strain, O. Farkas, D. K. Malick, A. D. Rabuck,
- K. Raghavachari, J. B. Foresman, J. V. Ortiz, Q. Cui, A. G. Baboul, S. Clifford, J. Cioslowski, B. B. Stefanov, G. Liu, A. Liashenko, P. Piskorz, I. Komaromi, R. L. Martin, D. J. Fox, T. Keith, M. A. Al-Laham, C. Y. Peng, A. Nanayakkara, M. Challacombe, P. M. W. Gill, B. Johnson, W. Chen, M. W. Wong, C. Gonzalez, J. A. Pople, GAUSSIAN 03 (revision C.02), Gaussian, Inc., Wallingford CT (USA) **2004**.
- [17] A. R. Williams, J. Kübler, C. D. Gelatt, *Phys. Rev. B*, 1979, 19, 6094; V. Eyert, *The Augmented Spherical Wave Method – A Comprehensive Treatment, Lecture Notes in Physics*, Springer, Berlin, Heidelberg, 2007.
- [18] V. Eyert, B. Siberchicot, M. Verdaguer, *Phys. Rev. B*, 1997, 56, 8959 – 8969.
- [19] G. Bester, M. Fähnle, J. Phys. Condens. Matter 2001, 13, 11541.
- [20] T. H. Dunning, Jr., P. J. Hay in Methods of Electronic Structure Theory, Modern Theoretical Chemistry, Vol. 3 (Ed.: H. F. Schaefer III), Plenum, New York, 1977, pp. 1–28.
- [21] P. J. Hay, W. R. Wadt, J. Chem. Phys. 1985, 82, 270.
- [22] M. Reiher, O. Salomon, B. A. Hess, *Theor. Chem. Phys.* 2001, 107, 48-55.
- [23] O. Salomon, M. Reiher, B. A. Hess, J. Chem. Phys. 2002, 117, 4729 – 4737.
- [24] M. Reiher, *Inorg. Chem.* **2002**, *41*, 6928 6935.